Feasibility of using coal as reinforcement in dissimilar welded joints: comparative analysis

Keegan J Zass[1], *Velaphi* Msomi[2*], *Sipokazi* Mabuwa[3]

[1]Cape Peninsula University of Technology, Faculty of Engineering and the Built Environment, Mechanical and Mechatronic Engineering, Bellville, 7535, South Africa.
[2]University of South Africa, College of Science, Technology, and Engineering, School of Engineering, Department of Mechanical Engineering, Florida Campus, South Africa.
[3]Durban University of Technology, Faculty of Engineering and the Built Environment, Mechanical and Mechatronic Engineering, Steve Biko Campus, Durban, 4000, South Africa.

Abstract. This study explores the possibility of using coal as reinforcement in dissimilar welded joints. The study involved joints of AA5083 and AA6082 alloys, which underwent friction stir welding (FSW), friction stir processing (FSP), and FSP with added coal powder (FSP+Coal). Microstructure analysis, microhardness testing, tensile tests, and fracture surface analysis were evaluated. The results indicated that FSP+Coal joints exhibited promising mechanical properties, with failure initiation at 130 MPa and a tensile strain of 6%, and complete failure at an ultimate tensile stress (UTS) of 144 MPa and a tensile strain of 9.5%. In comparison, FSP joints showed failure initiation at 130 MPa and a strain of 8.5%, and complete failure at 90 MPa and a strain of 14%. Additionally, FSP+Coal joints demonstrated a higher average hardness (8.3% higher than FSW joints and 4% higher than FSP joints), supported by fracture surface and microstructural analyses indicating a finer grain size of 13.15 μm in FSP+Coal joints, compared to 12.79 μm in FSP joints and 39.74 μm in FSW joints.

Keywords: Microstructure, dissimilar aluminium alloys, tensile strength, reinforced particles, microhardness.

1 Introduction

Friction Stir Processing (FSP) is a solid-state technique inspired by friction stir welding (FSW). It employs a rotating tool, comprising a pin and a shoulder, which applies pressure on the workpiece's outer surface while rotating at a specific speed [1-2]. FSP offers significant potential for improving material mechanical properties by eliminating various defects and refining microstructures. The rotational speed of the tool plays a crucial role in FSP, directly impacting heat generation during the process [3]. Furthermore, FSP has been adapted for the modification of microstructural arrangement of metals, where various base

* Corresponding author: msomiv@gmail.com

metals such as copper, iron, aluminium, and nickel, are used. By harnessing friction and heat, FSP effectively enhances material properties, providing a versatile means to enhance the characteristics of metals.

The manufacturing sector dedicated to producing aluminium-based products plays a crucial role in making various components like pistons, cylindrical blocks, brake drums, and other parts that endure high levels of wear, friction, and corrosion. Improved aluminium-based metals find applications in diverse industries such as aerospace, aviation, transportation, construction, marine, automotive, packaging, sports, and nuclear sectors. The improvement of aluminium-based metals involves the inclusion of foreign elements that can be introduced through casting or other methods. The improved aluminium-based metals make them suitable for various industrial applications like electrochemical, mechanical, structural, metallurgical, and isotopic applications [4-5].

In the typical manufacturing process, reinforcements are introduced into grooves or holes on the surface of a metal plate, followed by the application of FSP to amalgamate the two components. During FSP, a stirring tool is traversed through the material, effectively dispersing the reinforcement particles within the material. There are few works where FSP was employed to enhance the welded joint. This includes the work by Mabuwa and Msomi [6] where the dissimilar friction stir welded joints were subjected to the normal and submerged friction stir processing procedure. It was discovered that the FSP procedure impacted the microstructural arrangement significantly. It was further discovered that the environmental conditions also had an influence on the mechanical properties of the welded joint. The influence of FSP procedure on the mechanical properties of the tungsten inert gas (TIG) welded AA6061 and AA7075 was studied by Mehdi and Mishra [7]. The microstructural analysis showed a refined grain size post-FSP procedure. The defects that were observed in the TIG welded joint were completely eliminated by the FSP procedure. The mechanical properties of the friction stir processed joint were higher compared to the TIG welded joint.

Jesus et al. [8] investigated the impact of the FSP procedure on the fatigue strength of GMAW T-welded joints. The microscopic analysis showed a significant reduction of defects coupled with refined grains post-FSP procedure. It was further discovered that the fatigue life of the friction stir processed joint was significantly improved and this was attributed to the significant change that was brought by FSP procedure. A similar study was also conducted by Costa et al. [9]. However, these researchers employed FSP procedure on the metal inert gas (MIG) welded joints. It was discovered that the microstructural defects observed in MIG welded joints were eliminated post-FSP procedure. There was also a notable grain size refinement that were brought by the FSP procedure. There was also a significant improvement to the fatigue life of the joint post-FSP procedure and the improved fatigue life was attributed to the elimination of defects and the grain refinement.

Yang et al. [10] have investigated the impact of friction stir spot processing on the TA15TIG welded joints. The TIG welded joints were subjected to the single pass of friction stir spot processing and the resulting specimens were macrostructural and microstructurally analysed using scanning electron microscopy. It was discovered that the friction stir spot processed specimens possessed refined grains and this contributed to the enhanced mechanical properties when compared to the TIG welded joints. Liyakat and Veeman [11] have studied the impact of subjecting AA5052-H32 TIG welded joints to the FSP procedure. The microstructural analysis revealed that the microstructural arrangement was critically changed post-FSP procedure. The microstructural change resulted in improved mechanical properties.

It is very important to note that the employment of the FSP procedure to the welded joint has started to gain attention. However, there is not much that has been done in this aspect of material improvement hence the limited literature. It is further important to note that the employment of the FSP procedure is purely employed without incorporating any reinforcement. The current work is taking a step further studying the feasibility of incorporating coal (non-biodegradable material) during the application of the FSP procedure. The reinforced joints are studied comparatively with the normal processed joints with the purpose of recycling. This aspect of material improvement has never been explored.

2 Materials and Methods

For this study, AA5083-H111 and AA6082-T651 aluminium alloy plates, 6 mm thick, were utilized. Table 1 presents the chemical compositions of the plates that was measured using Belec Spectroscopy, while Table 2 provides the corresponding mechanical properties. No specific chemical or mechanical preparations were performed before cutting the plates. The dissimilar aluminium alloy plates were cut into dimensions of 70 × 530 × 6 mm, based on the dimensions of the FSW fixture. Friction stir welding (FSW) was initially conducted to join the two plates, resulting in three sets of FSW samples. Subsequently, the three sets of friction stir welded joints underwent friction stir processing with and without coal inclusion. The friction stir welding and friction stir processing were performed using the converted Lagun FU.1-LA: A versatile universal milling machine. During the FSW, the AA5083-H321 plate was positioned on the advancing side, while the AA6082-T651 plate was positioned on the retreating side of the tool. This configuration was maintained for FSP and FSP+Coal. Table 3 outlines the friction stir welding and friction stir processing parameters employed to join and process the dissimilar aluminium joints. Table 4 presents the chemical compositions of the coal powder.

Table 1. Nominal chemical composition base material alloy 5083 and alloy 6082 [5].

Material	Mn	Fe	Cu	Mg	Si	Zn	Cr	Ti	Al
AA5083	0.616	0.173	0.016	4.238	0.131	0.017	0.039	0.010	Balance
AA6082	0.83	0.49	0.14	1.04	1.03	0.186	0.237	0.06	Balance

Table 2. Mechanical properties of aluminium alloy 5083 H111 and 6082 T651.

Property	Value	
	AA5083 H111	**AA6082 T651**
Ultimate Tensile Strength (UTS)	300 MPa	340 MPa
Elongation	23 %	11%
Hardness Vickers	75 HV	100 HV

Figure 1 depicts the dimensions of the tool utilized in both FSW and FSP procedures. Figure 2 showcases the arrangement of AA5083-H111 and AA6082-T651 plates for FSW, FSP, and FSP+Coal. Specifically, Figure 2(a) exhibits the FSW configuration, while Figure 2(b) illustrates the FSP setup without reinforcement. Figures 2(c) to 2(f) elaborate on the FSP+Coal setup. In this process, finely crushed organic braai coal acted as reinforcement particles. Holes, measuring 2 mm in diameter and 5.8 mm deep, were drilled at 5 mm intervals across the 530 mm FSW plate. Equal amounts of coal powder were inserted into these holes (Figure 2(c)). After inserting manually crushed coal (Figure 2(d)) into the joint, a pin-less FSP tool was employed to cover the holes to prevent splashing (Figure 2(e)). Subsequently, the tool with a pin was utilized for a single-pass FSP process along with pre-

drilled blind holes on the same joint, depicted in Figure 2(f). The resulting dissimilar joints for FSW, FSP, and FSP+Coal are displayed in Figures 3(a) to 3(c), respectively.

Table 3. FSW/FSP parameters.

Rotational speed	**Traverse speed**	**Tilt angle**
1200 rpm	40 mm/min	2º

Table 4: Chemical composition of coal

	Coal Powder % Present		
Chemical Element	Carbon	Oxygen	Total
Measurement 1	93.85	6.15	100
Measurement 2	78.42	21.58	100
Measurement 3	89.78	10.22	100
Measurement 4	84.1	15.9	100
Measurement 5	76.46	23.54	100
Measurement 6	73.21	26.79	100
Mean	82.64	17.36	100
Std. deviation	8.05	8.05	

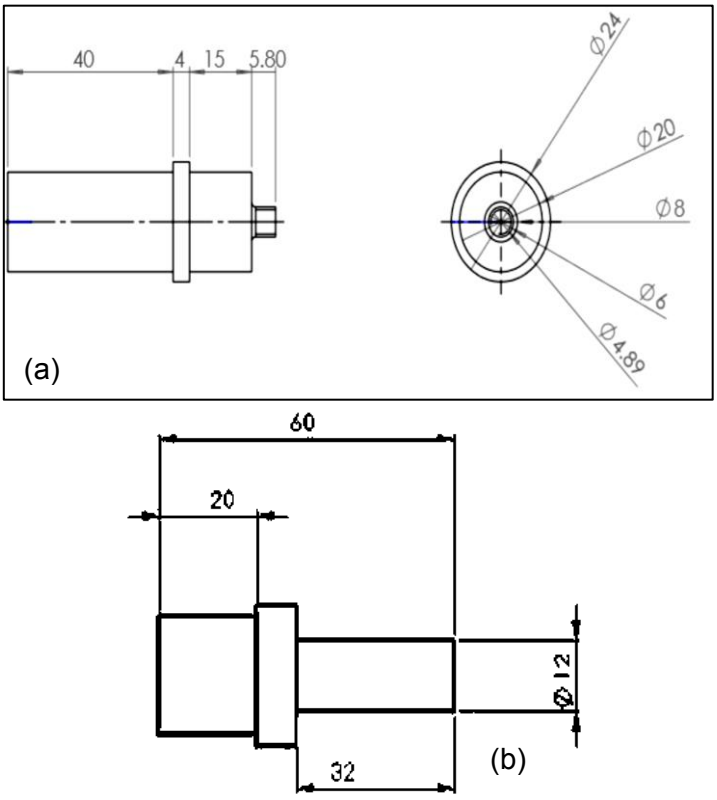

Fig. 1. (a) FSW/FSP tool, and (b) FSP pinless.

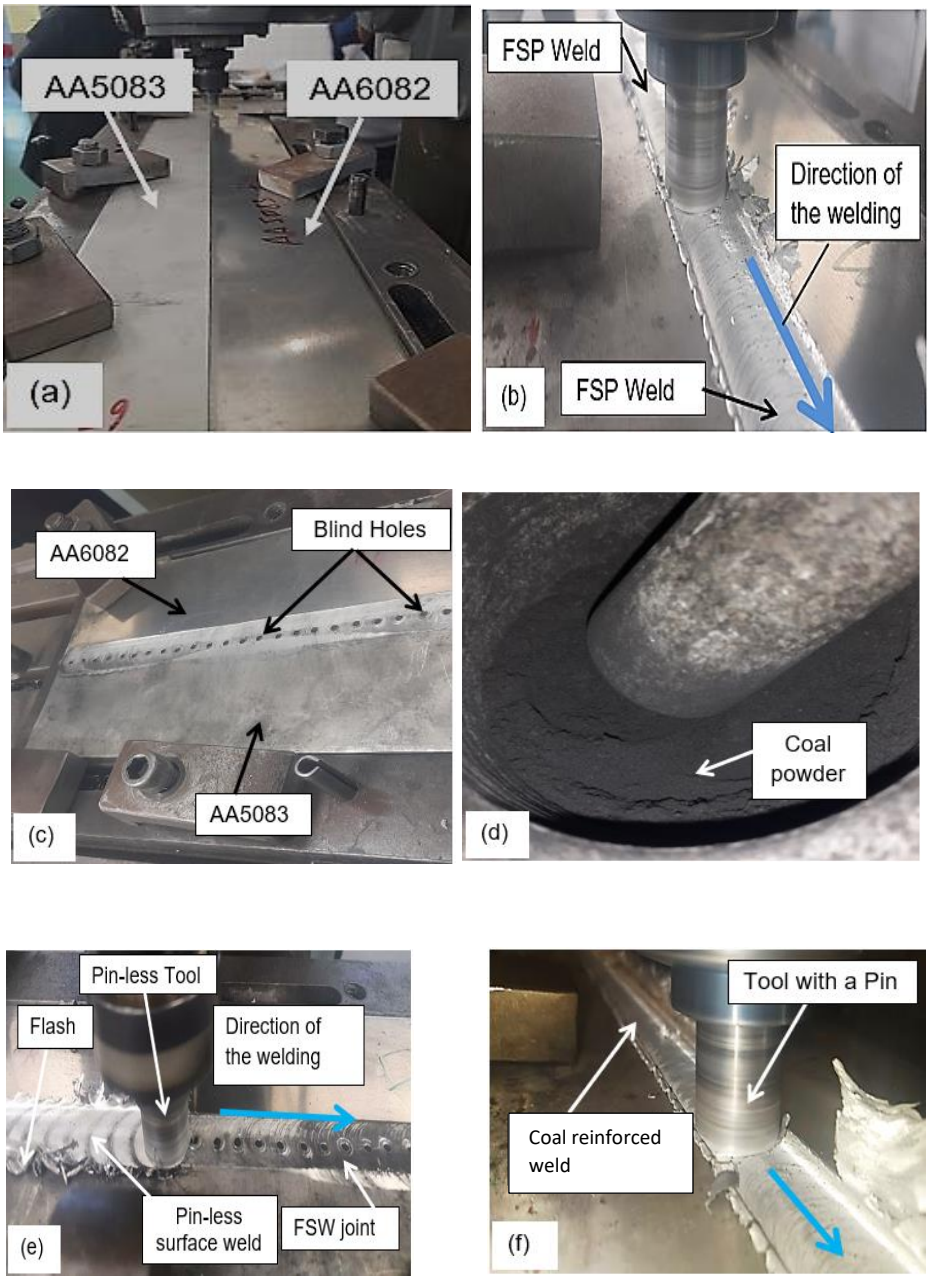

Fig. 2: Setup, (a) FSW, (b) FSP, (c) FSP with blinds holes for coal powder. (d) Crushed coal (e) Enclosing coal using a pin-less tool, (f) FSP using a tool with a pin.

The tests performed encompassed macrostructure analysis, microstructure analysis, tensile testing, fracture surface analysis, and microhardness testing. For microstructural analysis (depicted in Figure 4(a)), specimens were embedded in thermosetting plastic after cutting to facilitate handling. These embedded samples underwent grinding, polishing, and etching using Weck's reagent, comprising 95 ml distilled water, 1.5 ml HCl, 1.0 ml HF, and 2.5 ml HNO_3. Microstructural images of FSW joints were captured using the Motic AE2000

metallurgical light optical microscope, assisted by Motic Images Plus 3.0 software. The analysis of the base material employed a 20x objective lens, and the captured images were analyzed using the line intercept method via ImageJ software.

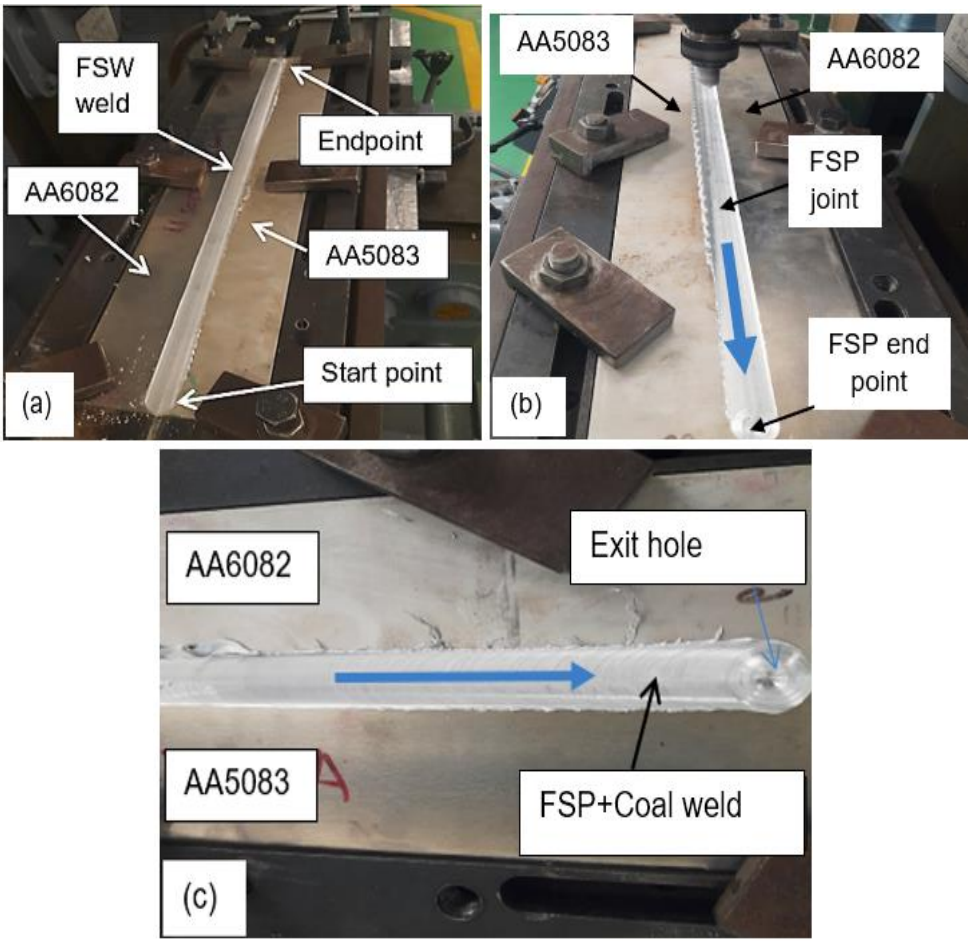

Fig. 3: Produced dissimilar aluminium joints (a) FSW, (b) FSP, and (c) FSP+Coal

Tensile testing was carried out using the Hounsfield 50K testing machine, which was equipped with Horizon software, following the specimen geometry and testing protocols specified in the ASTM E8M-04 standard. Figure 4(b) presents the dimensions of the tensile specimen in millimeters. Microhardness tests were conducted using the Falcon 5000 Innovatest hardness testing machine with IMPRESSIONS software, following the guidelines outlined in the ASTM E384-11 standard. The test parameters included a 0.3 kg load, a 1 mm spacing between indents, and a total of 25 measurement indents. Figure 4(c) demonstrates three sets of readings obtained per specimen, employing the 10× and 20× objectives for precise specimen focusing and accurate measurements.

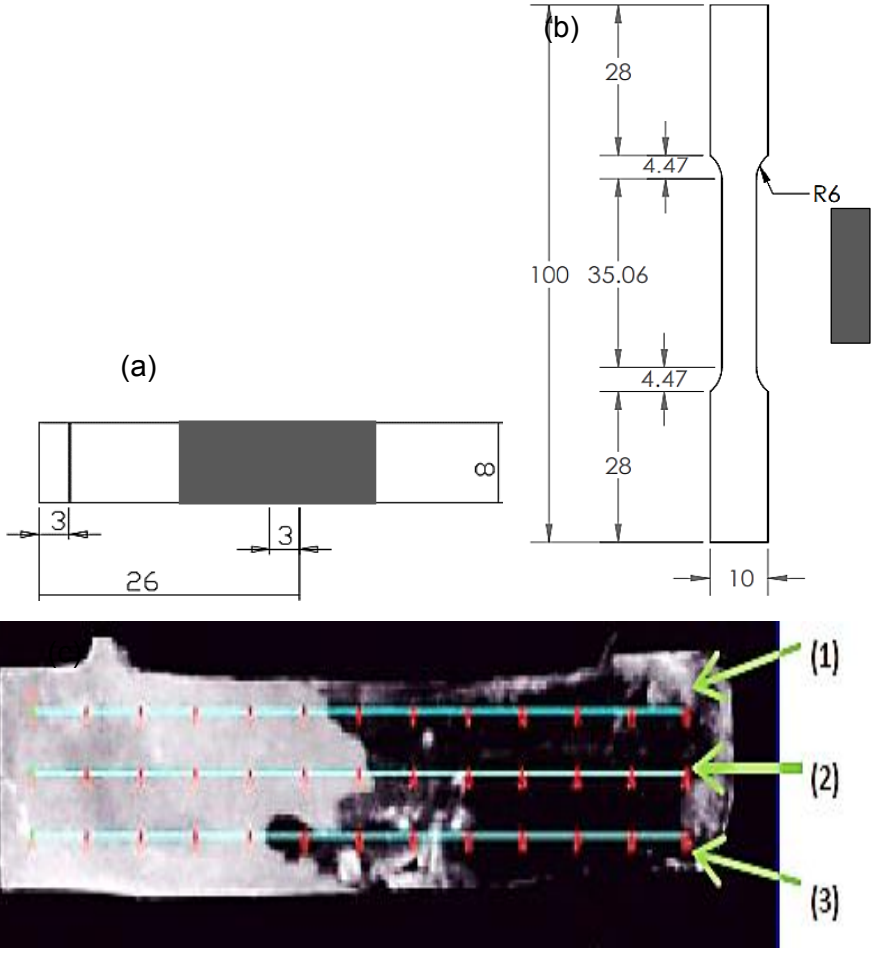

Fig. 4: (a) Microstructure/ microhardness specimen, (b)Tensile specimen, and (c) Sample – microhardness indentation.

3 Results and Discussion

3.1 Macrostructure and Microstructure

Figure 5 illustrates the FSW, FSP, and FSP+Coal welded joints. In the first set of macrographs (Figure 5(a)), the FSW joints exhibit small visible defects, notably a tunnel defect highlighted by a yellow circle. Similarly, the FSP samples display tunnel defects due to insufficient heat and material flow during initial joint formation [12-13]. The use of dissimilar alloys with distinct melting points causes AA5083 to soften before AA6082, resulting in inadequate material mixing and microstructural defects, as seen in Figure 5(b) [14-15]. Additionally, Figure 5(c) depicts friction stir processing with coal reinforcement (FSP+Coal), where a sample marked with a yellow circle also displays a tunnel defect in the nugget zone, akin to the one observed in the FSP sample.

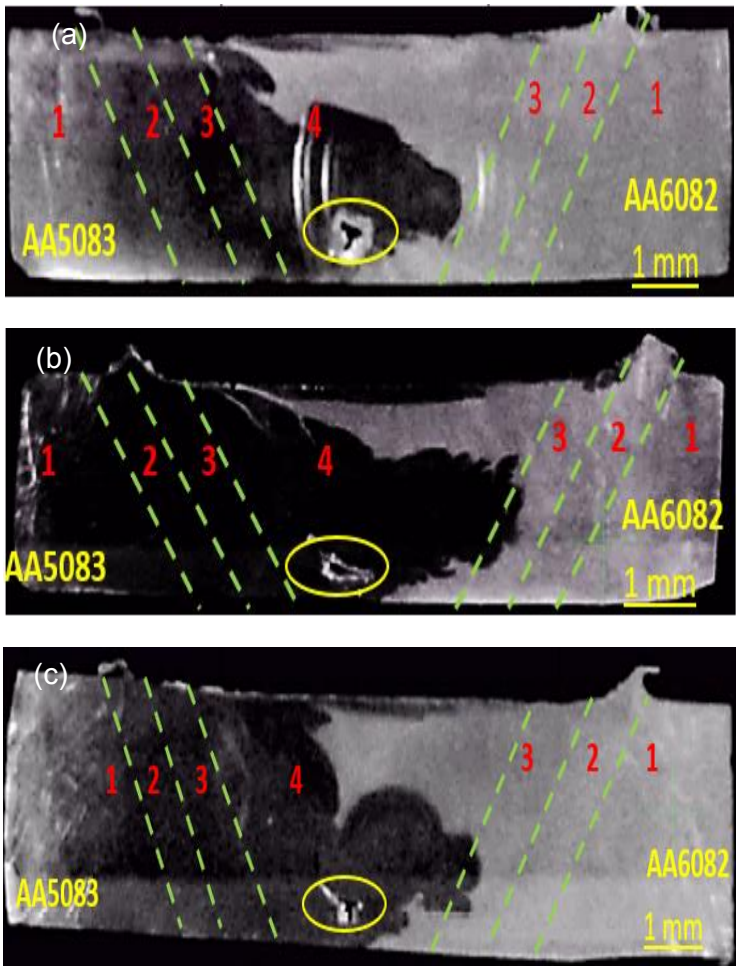

Fig. 5. Macrographs, (a) FSW, (b) NFSP, and (c) FSP + Coal.

Microstructural analysis of the welded samples involved metallographic tests on transverse cross-sections. Figures 6(a-c) show micrographs captured specifically from the stir zones of the FSW, FSP, and FSP+Coal welded joints at their midpoint positions. Table 4 summarizes the grain sizes depicted in Figure 6: in Figure 6(a), the FSW welded joints display a fully recrystallized grain structure with distinct boundary layers, resulting in significantly smaller grain size compared to the AA6082 parent material (PM). Figure 6(b) reveals the processed FSP grain structure with finer grains than FSW, credited to intense plastic deformation caused by the rotating tool in the stir zone, leading to micro-constituent breakdown and partial recrystallization. In Figure 6(c), the FSP+Coal sample displays the smallest grain sizes at 12.789 μm, almost comparable to FSP. These observations shed light on the varied microstructural features resulting from different processing techniques, emphasizing the impact of plastic deformation and recrystallization on the grain structure of welded joints [16-17].

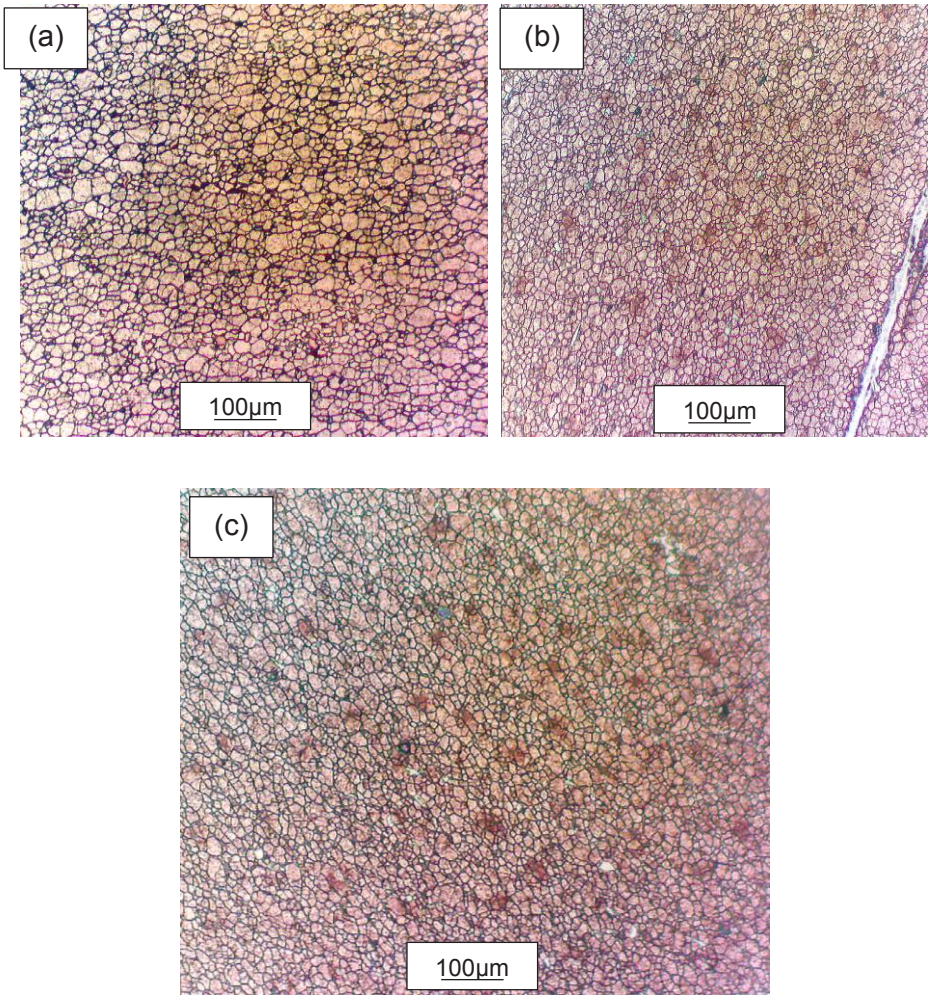

Fig. 6. Stir zone micrographs, (a) FSW, (b) NFSP, and (c) FSP+Coal.

Table 4: Grain sizes of the stir zones.

Joint	Mean grain size (µm)	Standard deviation (µm)
FSW	39.743	16.814
FSP	13.145	5.119
FSP+Coal	12.789	4.211

3.2. Tensile properties

Figure 7 displays the processed specimens of FSWed, FSPed, and FSP+Coal joints post-tensile testing. In both FSWed and FSPed specimens, failure occurred outside the welded area in the Heat-Affected Zone (HAZ) of the AA6082 side, evident in the reduced area due to necking (Figure 7(a-b)). This outer joint failure, specifically in the HAZ, signifies a seamless joint and indicates the joint's strength surpasses that of AA6082 [18]. The consistent occurrence of failure outside the joint in both FSW and FSP specimens highlights the joint's strength relative to the AA6082 side, with the HAZ exhibiting the lowest strength, a typical phenomenon in dissimilar material joining [19-22].

In the case of FSP+Coal, failure occurred within the welding zone, close to the AA5083 side, exhibiting a brittle nature. Specifically, the failure took place at the thermomechanically affected zone (TMAZ) without any signs of elongation or ductility, indicating a brittle failure [23]. This type of failure suggests a significant influence of the coal powder material, leading to failure within the welded area, as depicted in Figure 7(c). Notably, the failure did not occur at the center of the specimen but rather in the vicinity of the coal powder presence.

Figure 7(d) illustrates the tensile stress-strain curves for the FSWed, FSPed joints, and FSP+Coal reinforcement particles. The corresponding tensile properties are provided in Table 5, which is also depicted in Figure 7. The FSWed joints showed a maximum Ultimate Tensile Stress (UTS) of 166.6 MPa, accompanied by a corresponding tensile strain rate of 9.28%. The FSPed joints displayed a maximum UTS of 126.66 MPa at a corresponding tensile strain rate of 9.14%. Conversely, the FSP+Coal joints exhibited a maximum UTS of 142 MPa, paired with a corresponding tensile strain rate of 9.28%.

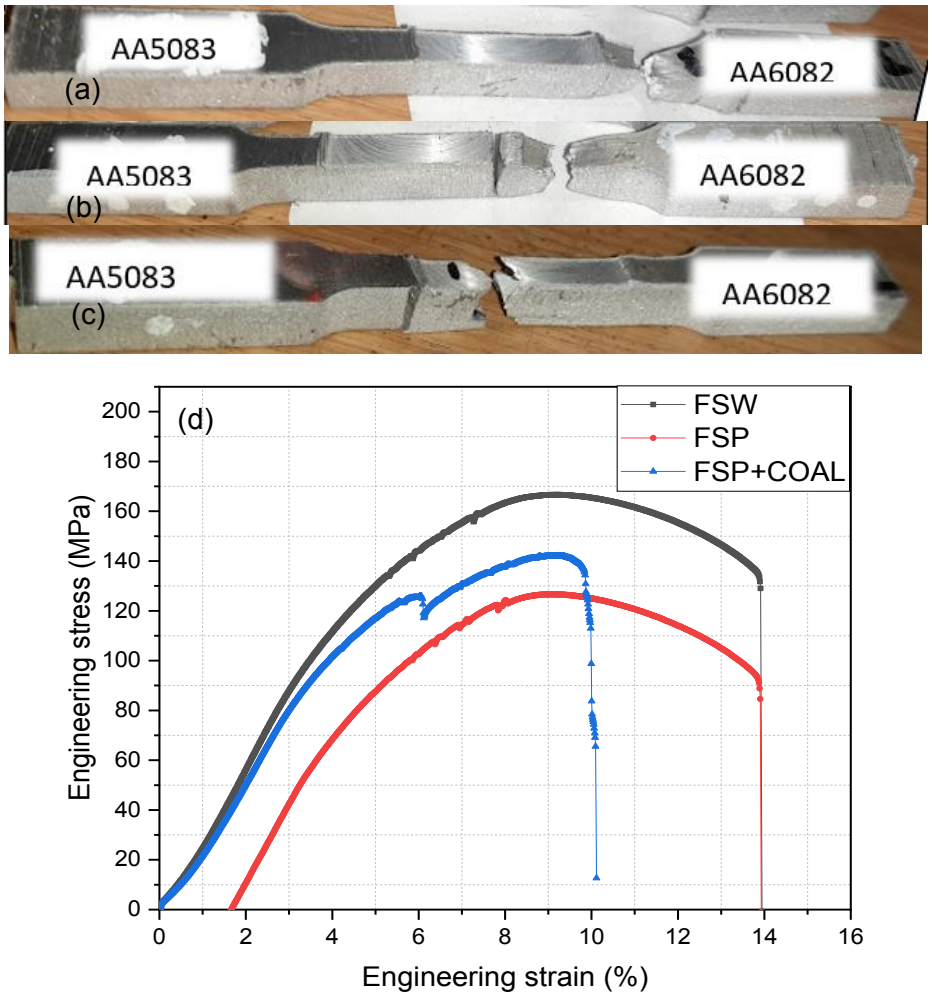

Fig. 7. Post tensile specimens (a) FSW, (b) FSP, (c) FSP+Coal specimen, and (d) Tensile stress-strain curves.

Table 5. Tensile properties joints results.

Sample	Ultimate Tensile Stress (MPa)	Tensile strain at UTS(%)	Tensile strain at breakpoint (%)	Position of fracture
FSW	166.6	9.28	13.9	HAZ/AA5083
FSP	126.66	9.14	13.9	HAZ/AA5083
FSP+Coal	142	9.28	10.09	TMAZ/AA6082

3.3 Fractographic analysis

Figure 8 displays the fracture surface morphology of the FSW, FSP, and FSP+Coal welding joints, revealing numerous circular dimples of varying sizes, indicative of a pronounced ductile failure mechanism. Tensile specimen analysis confirmed the predominantly ductile nature of the joint fracture mode. In FSW and FSP, the failure occurred at the AA5083 side, while FSP+Coal led to failure on the AA6082 side. The joints' ductility was evident from characteristic features such as diverse-sized dimples, as supported by previous studies [20,24-26]. The figure highlights specific elements of ductile characteristics, including inclusion particles (green arrow), intergranular fractures (yellow), trans-granular cleavage facets and micro dimples (red arrow), and micro-voids (blue arrow).

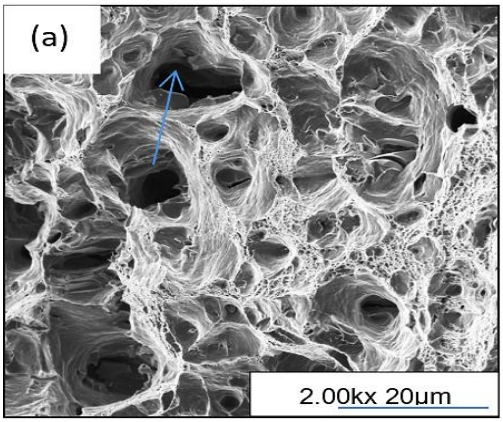

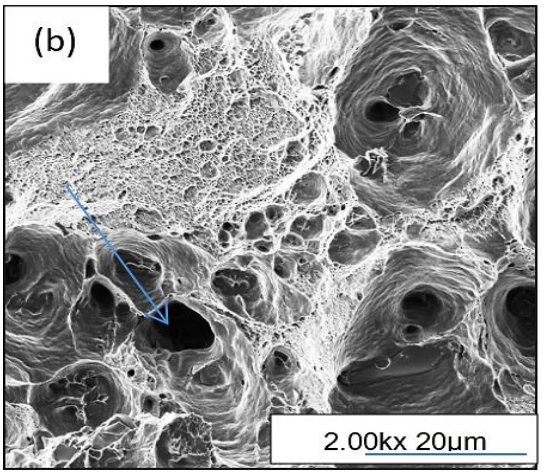

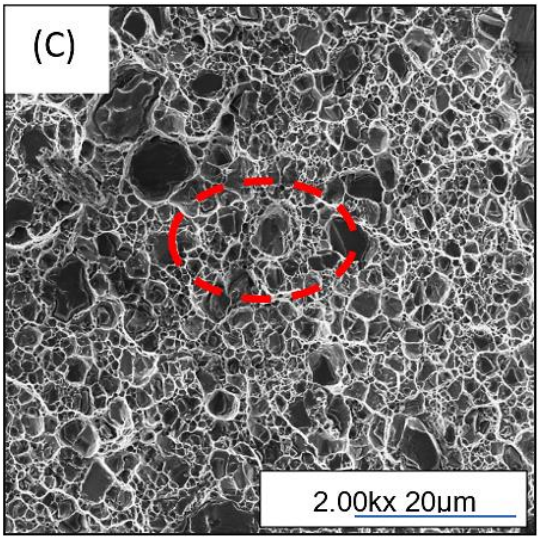

Fig. 8. Fractography, (a) FSW, (b) FSP, and (c) FSP-Coal.

3.4 Hardness analysis

Figure 9 presents the Vickers hardness profiles for FSW-welded, FSP, and FSP+Coal joints at various positions. Additionally, Figure 9(d) shows the NZ hardness bar charts for these joints. The results indicated that AA5083 H111 consistently exhibited higher hardness values than AA6082 T51 in all conducted tests. Notably, FSW, FSP, and FSP+Coal joints displayed higher hardness values than AA6082 T651 at the nugget zone, averaging between 55-75 HV0.3 throughout the weld positions in FSW (Figure 9(a)). Hardness values decreased across all welded joints towards AA6082-T651. Moreover, minimal differences were observed between the tool shoulder and tool pin positions on the AA5083-H111 edges compared to the nugget zones, especially at the initial and middle weld positions. At the end of the weld, the tool shoulder edges exhibited higher values than the nugget zone.

Positions near the tool pin and tool shoulder areas on the AA6082-T651 side exhibited relatively lower hardness values compared to other regions. However, the nugget zone displayed a significant increase in hardness values across the entire length of the welded joint, surpassing the hardness of the AA6082-T651 Heat-Affected Zone (HAZ) side. This hardness increase is attributed to the fine grain size generated by the FSW process and the work-hardening effect induced during the process, as documented in [27]. The AA6082 alloy, being a precipitate-hardened alloy, is significantly affected by temperatures above 200°C, impacting its properties [28-29]. The data below indicates that the temperature has notably influenced the AA6082 alloy, especially on the HAZ side, in comparison to the AA6082 T651 base material.

The results depicted in Figure 9(b) reveal that FSP achieved a maximum hardness of 95 HV at the nugget zone with a single pass, while the maximum hardness at TMAZ was 85 HV, decreasing to 54 HV at the beginning of the AA6082 base metal. This indicates that the processed joints exhibit enhanced resistance to deformation. The hardness behaviour observed in FSP aligns with that of wrought 5XXX series aluminium alloys, displaying minimal hardness variation between the nugget zone and the base material [30-35]. This finding is consistent with the tensile strength results of FSW and FSP presented in section

3.2, suggesting grain size refinement in the processed joint. However, it's noteworthy that the tensile failure and bending occurred on the AA6082 side.

In this section, the hardness tests performed on FSP+Coal welded joints are presented, as shown in Figure 9(c). The hardness values of AA5083 H111 at the tool shoulder on the AA5083-H111 edges showed minimal variation compared to the nugget zones, with a maximum hardness value of 84 HV. Additionally, all three welded depth lines were closely clustered together as they extended from AA5083-H111 through the nugget zone to the AA6082-T651 side, which contrasts with the depth lines observed in FSW and FSP.

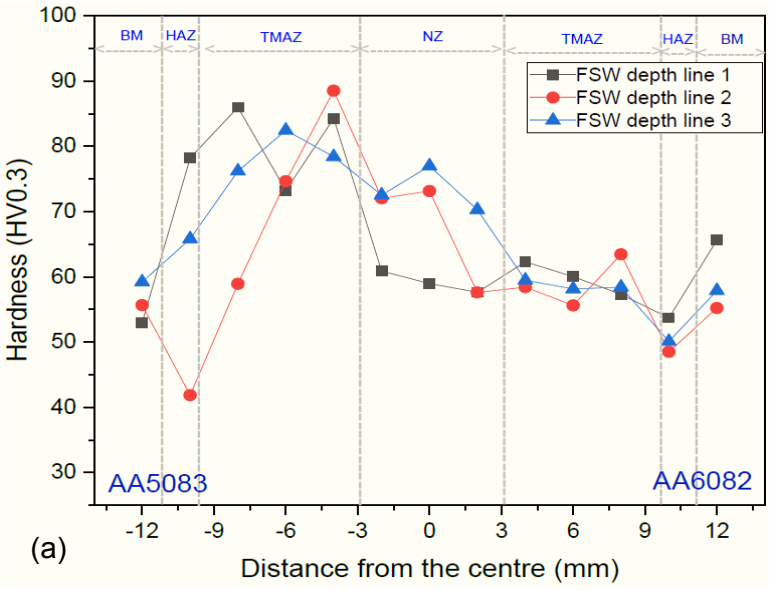

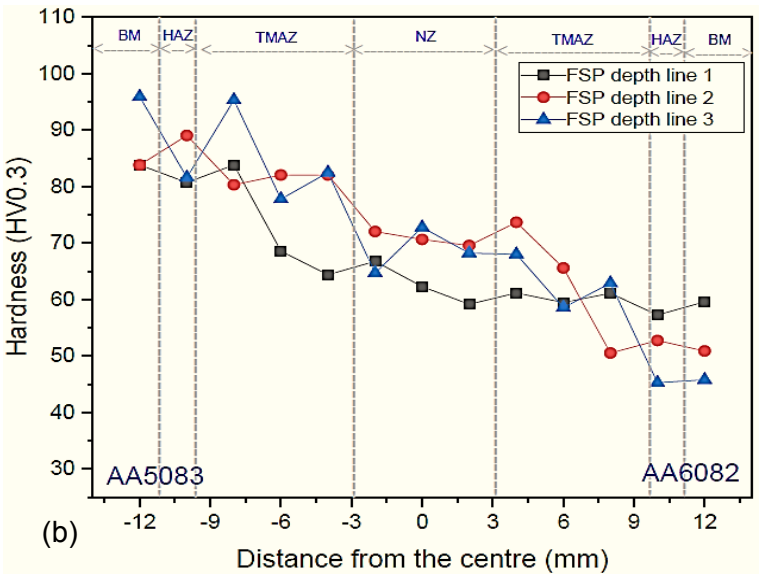

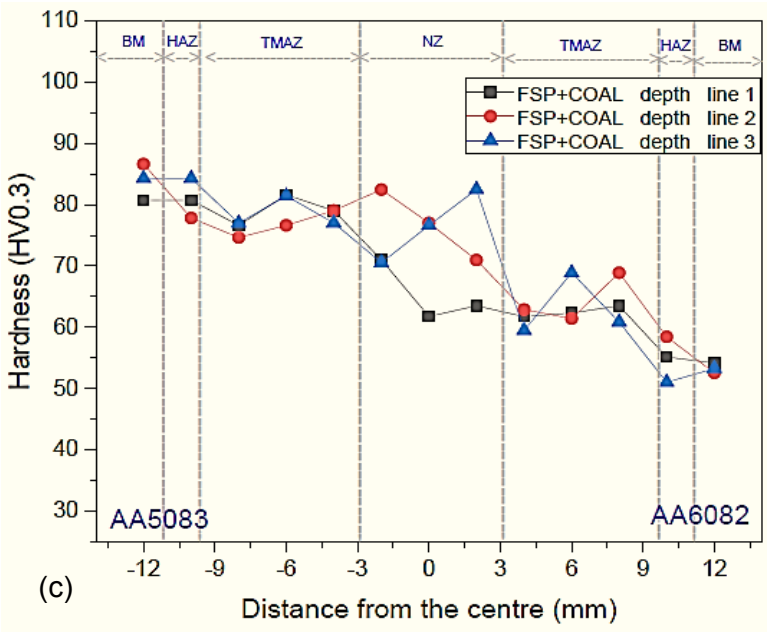

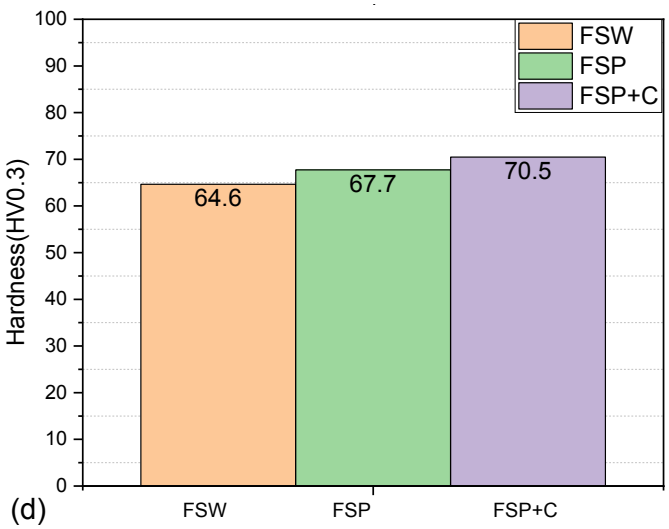

Fig. 9. Microhardness profiles: (a) FSW, (b) FSP, (c) FSP+Coal; (d) Average SZ microhardness charts.

4 Conclusions

This study comprehensively analyzed the FSW, FSP, and FSP+Coal joints under general conditions, exploring the potential enhancement of mechanical properties in FSP welded joints by incorporating coal powder. The resulting conclusions stem from the study's findings.

The findings demonstrate that the mechanical properties of the processed FSP+Coal welded joints are superior to those of the parent material and FSP joints. This improvement is evident

in the tensile stress-strain curves, revealing that FSP+Coal joints exhibit a more favourable curve. Specifically, these joints begin to fail at 130 MPa with a strain of 6% and completely fail at an Ultimate Tensile Stress of 144 MPa with a strain of 9.5%. In contrast, FSP joints start failing at 130 MPa with a strain of 8.5% and completely fail at 90 MPa with a strain of 14%. Additionally, the hardness of FSP+Coal was on average 8.3% higher than FSW and 4% higher than FSP. The results suggest that FSP+Coal joints can be further optimized by adjusting welding parameters such as welding speed, rotation speed, and tilting angle to achieve better results. These findings offer valuable insights for the development and optimization of FSP joints reinforced with coal powder.

5 Acknowledgment

The authors would like to thank the Mechanical and Mechatronic Engineering Workshop staff for assisting with some practicals. The authors would like to declare that ChatGPT was used to correct grammar in some parts of this paper.

References

1. Mishra, R.S., Mahoney, M.W., McFadden, S.X., Mara, N.A., Mukherjee, A.K.,1999. High strain rate superplasticity in a friction stir processed 7075 Al alloy, *Scripta Materialia*, 42(2), pp. 163-168.
2. Mishra, R.S., and Ma, Z.Y., 2005. Friction stir welding and processing, *Materials Science and Engineering: R: Reports*, 50(1–2), pp. 1-78.
3. Yang, Q., Xiao, B.L., Ma, Z.Y., 2013. Enhanced superplasticity in friction stir processed Mg–Gd–Y–Zr alloy, *Journal of Alloys and Compounds*, 551, pp. 61-66
4. Wang, G., Zhao, Y., Hao, Y., 2018. Friction stir welding of high-strength aerospace aluminum alloy and application in rocket tank manufacturing, *Journal of Materials Science & Technology*, 34(1), pp. 73-91.
5. Abioye, T.E., Zuhailawati, H., Aizad, S., Anasyida, A.S., 2019. Geometrical, microstructural and mechanical characterization of pulse laser welded thin sheet 5052-H32 aluminium alloy for aerospace applications, *Transactions of Nonferrous Metals Society of China*, 29(4), pp. 667-679.
6. Mabuwa, S. and Msomi, V., 2020. Comparative analysis between normal and submerged friction stir processed friction stir welded dissimilar aluminium alloy joints. *Journal of Materials Research and Technology*, *9*(5), pp.9632-9644.
7. Mehdi, H. and Mishra, R.S., 2021. Effect of friction stir processing on mechanical properties and heat transfer of TIG welded joint of AA6061 and AA7075. *Defence Technology*, *17*(3), pp.715-727.
8. Jesus, J.S., Costa, J.M., Loureiro, A. and Ferreira, J.M., 2017. Fatigue strength improvement of GMAW T-welds in AA 5083 by friction-stir processing. *International Journal of Fatigue*, *97*, pp.124-134.
9. Costa, J.D.M., Jesus, J.S., Loureiro, A., Ferreira, J.A.M. and Borrego, L.P., 2014. Fatigue life improvement of mig welded aluminium T-joints by friction stir processing. *International journal of fatigue*, *61*, pp.244-254.
10. Yang, X.W., Li, W.Y., Li, H.Y., Yao, S.T., Sun, Y.X., Sun, Y.X. and Lu, M.E.I., 2018. Microstructures and microhardness for sheets and TIG welded joints of TA15 alloy using friction stir spot processing. *Transactions of Nonferrous Metals Society of China*, *28*(1), pp.55-65.

11. Liyakat, N.A. and Veeman, D., 2022. Improvement of mechanical and microstructural properties of AA 5052-H32 TIG weldment using friction stir processing approach. *Journal of Materials Research and Technology*, *19*, pp.332-344.
12. Derazkola, H.A., Eyvazian, A. and Simchi, A., 2020. Submerged friction stir welding of dissimilar joints between an Al-Mg alloy and low carbon steel: Thermo-mechanical modeling, microstructural features, and mechanical properties. *Journal of Manufacturing Processes*, *50*, pp.68-79.
13. Huang, G., Wu, J., Hou, W. and Shen, Y., 2018. Microstructure, mechanical properties and strengthening mechanism of titanium particle reinforced aluminum matrix composites produced by submerged friction stir processing. *Materials Science and Engineering: A*, *734*, pp.353-363.
14. Ramaiyan, S., Santhanam, S.K.V. and Muthuguru, P., 2018. Effect of scroll pin profile and tool rotational speed on mechanical properties of submerged friction stir processed AZ31B magnesium alloy. *Materials Research*, *21*, p.e20170769.
15. Yan B, Li H, Zhang J, Kong N. The Effect of Initial Annealing Microstructures on the Forming Characteristics of Ti–4Al–2V Titanium Alloy. *Metals*. 2019; 9(5):576.
16. Subramani, V., Jayavel, B., Sengottuvelu, R. and Lazar, P.J.L., 2019. Assessment of microstructure and mechanical properties of stir zone seam of friction stir welded magnesium AZ31B through nano-SiC. *Materials*, *12*(7), 1044.
17. Prosgolitis, C.G., Lambrakos, S.G. and Zervaki, A.D., 2018. Phase-field modeling of nugget zone for a AZ31-Mg-alloy friction stir weld. *Journal of Materials Engineering and Performance*, *27*, pp.5102-5113.y
18. Sathari, N.A.A., Razali, A.R., Ishak, M. and Shah, L.H., 2015. Mechanical strength of dissimilar AA7075 and AA6061 aluminum alloys using friction stir welding. *International Journal of Automotive and Mechanical Engineering*, *11*, 2713.
19. Msomi, V. and Mbana, N., 2020. Mechanical properties of friction stir welded AA1050-H14 and AA5083-H111 joint: sampling aspect. *Metals*, *10*(2), 214.
20. Mabuwa, S. and Msomi, V., 2021. The effect of FSP conditions towards microstructure and mechanical properties of the AA6082/AA8011 TIG-welded joint. *Materials Research Express*, *8*(6), p.066514.
21. Kopyściański, M., Węglowska, A., Pietras, A., Hamilton, C. and Dymek, S., 2016. Friction stir welding of dissimilar aluminum alloys. *Key Engineering Materials*, *682*, pp.31-37.
22. KumarSingh, S., Tiwari, R.M., Kumar, S. and Kumar, S., 2018. Mechanical properties and micrstructure of Al-5083 by TIG. *Materials Today: Proceedings*, *5*(1), pp.819-822.
23. Sameer, M.D. and Birru, A.K., 2019. Mechanical and metallurgical properties of friction stir welded dissimilar joints of AZ91 magnesium alloy and AA 6082-T6 aluminium alloy. *Journal of Magnesium and Alloys*, *7*(2), pp.264-271.
24. Yang, S., Yang, X., Lu, X., Li, M., Zuo, H. and Wang, Y., 2023. Strength calculation and microstructure characterization of HAZ softening area in 6082-T6 aluminum alloy CMT welded joints. *Materials Today Communications*, p.107077.
25. Xu, X., Zhu, W., Guo, X., Liang, C. and Deng, Y., 2023. Effect of ageing treatment process on the microstructure development and mechanical properties of 6082 Al alloy. *Journal of Alloys and Compounds*, *935*, p.167892.
26. Zhao, W., Liu, R.F., Yan, J., Wang, X., Zhang, H.W. and Wang, W.X., 2022. Overall optimization in microstructure and mechanical properties of 5 wt% SiC/7075Al composites by high-frequency electric pulse assisted treatment. *Journal of Materials Research and Technology*, *21*, pp.2156-2167.
27. Hussein, W. and Al-Shammari, M.A., 2018, December. Fatigue and fracture behaviours of FSW and FSP joints of AA5083-H111 aluminium alloy. In *IOP Conference Series: Materials Science and Engineering* (Vol. 454, No. 1, p. 012055). IOP Publishing.

28. Sameer, M.D. and Birru, A.K., 2019. Mechanical and metallurgical properties of friction stir welded dissimilar joints of AZ91 magnesium alloy and AA 6082-T6 aluminium alloy. *Journal of Magnesium and Alloys*, *7*(2), pp.264-271.
29. Kosturek, R., Torzewski, J., Wachowski, M. and Śnieżek, L., 2022. Effect of Welding Parameters on Mechanical Properties and Microstructure of Friction Stir Welded AA7075-T651 Aluminum Alloy Butt Joints. *Materials*, *15*(17), p.5950.
30. Mehdi, H. and Mishra, R.S., 2020. Influence of friction stir processing on weld temperature distribution and mechanical properties of TIG-welded joint of AA6061 and AA7075. *Transactions of the Indian Institute of Metals*, *73*, pp.1773-1788.
31. Wei, J., He, C., Zhao, Y., Qie, M., Qin, G. and Zuo, L., 2023. Evolution of microstructure and properties in 2219 aluminum alloy produced by wire arc additive manufacturing assisted by interlayer friction stir processing. *Materials Science and Engineering: A*, *868*, p.144794.
32. He, P., Bai, X. and Zhang, H., 2023. Microstructure refinement and mechanical properties enhancement of wire and arc additively manufactured 6061 aluminum alloy using friction stir processing post-treatment. *Materials Letters*, *330*, p.133365.
33. Paidar, M., Vignesh, R.V., Khorram, A., Ojo, O.O., Rasoulpouraghdam, A. and Pustokhina, I., 2020. Dissimilar modified friction stir clinching of AA2024-AA6061 aluminum alloys: Effects of materials positioning. *Journal of Materials Research and Technology*, *9*(3), pp.6037-6047.
34. Msomi, V. and Moni, V., 2022. The influence of materials positioning on microstructure and mechanical properties of friction stir welded AA5083/AA6082 dissimilar joint. *Advances in Materials and Processing Technologies*, *8*(2), pp.2087-2101.
35. Mabuwa, S., Msomi, V., Mehdi, H. and Saxena, K.K., 2023. Effect of material positioning on Si-rich TIG welded joints of AA6082 and AA8011 by friction stir processing. *Journal of Adhesion Science and Technology*, *37*(17), pp.2484-2502.